Computer Physics Communications 185 (2014) 2034–2045

Contents lists available at ScienceDirect

Computer Physics Communications

journal homepage: www.elsevier.com/locate/cpc

Accurate finite element modeling of acoustic waves

A. Idesman *, D. Pham

Department of Mechanical Engineering, Texas Tech University, Lubbock, TX 79409-1021, USA

ARTICLE INFO

Article history:
Received 3 May 2013
Received in revised form
8 April 2014
Accepted 10 April 2014
Available online 18 April 2014

Keywords:
Acoustic waves
Numerical dispersion
Explicit time integration
Finite elements

ABSTRACT

In the paper we suggest an accurate finite element approach for the modeling of acoustic waves under a suddenly applied load. We consider the standard linear elements and the linear elements with reduced dispersion for the space discretization as well as the explicit central-difference method for time integration. The analytical study of the numerical dispersion shows that the most accurate results can be obtained with the time increments close to the stability limit. However, even in this case and the use of the linear elements with reduced dispersion, mesh refinement leads to divergent numerical results for acoustic waves under a suddenly applied load. This is explained by large spurious high-frequency oscillations. For the quantification and the suppression of spurious oscillations, we have modified and applied a two-stage time-integration technique that includes the stage of basic computations and the filtering stage. This technique allows accurate convergent results at mesh refinement as well as significantly reduces the numerical anisotropy of solutions. We should mention that the approach suggested is very general and can be equally applied to any loading as well as for any space-discretization technique and any explicit or implicit time-integration method.

1. Introduction

In the paper we will consider the propagation of acoustic waves in an isotropic homogeneous medium described by the following scalar wave equation:

$$\frac{\partial^2 u}{\partial t^2} - c_o^2 \nabla^2 u = f, \tag{1}$$

where u is the field variable, c_o is the wave velocity, f is the body force, and t is the time. The application of the space discretization to Eq. (1) leads to a system of ordinary differential equations in time

$$\boldsymbol{M}\,\ddot{\boldsymbol{U}} + \boldsymbol{K}\,\boldsymbol{U} = \boldsymbol{R}, \tag{2}$$

where $\boldsymbol{M}$ and $\boldsymbol{K}$ are the mass and stiffness matrices, respectively, $\boldsymbol{U}(t)$ is the vector of the nodal field variable, and $\boldsymbol{R}(t)$ is the vector of the nodal load. Due to the space discretization, the exact solution to Eq. (2) contains the numerical dispersion error; e.g., see [1–15] and others. The space discretization error can be decreased by the use of mesh refinement. However, this procedure significantly increases computational costs. Therefore, special techniques have been developed for the reduction in the numerical dispersion error which is also related to "the pollution effect" (e.g., see [16–18] and others for the study of the pollution error). One simple and effective technique for acoustic and elastic wave propagation problems is based on the calculation of the mass matrix $\boldsymbol{M}$ in Eq. (2) as a weighted average of the consistent and lumped mass matrices; see [5–8] and others. For the 1-D case and linear finite elements, this approach reduces the error in the wave velocity for harmonic waves from the second order to the fourth order of accuracy. However, for harmonic wave propagation in the 2-D and 3-D cases, these results are not valid (nevertheless, in the multi-dimensional case, the averaged mass matrix yields more accurate results compared with the standard mass matrix). We should also mention that the known publications on the techniques with the averaged mass matrix do not include the effect of finite time increments on the dispersion error and on the accuracy of the numerical

* Corresponding author. Tel.: +1 806 834 2606; fax: +1 806 742 3540.
E-mail addresses: alexander.idesman@coe.ttu.edu, alexander.idesman@ttu.edu (A. Idesman).

http://dx.doi.org/10.1016/j.cpc.2014.04.009
0010-4655/

results. As shown in the current paper, if we use the weighting coefficients for the averaged mass matrix that are independent of time increments (as in the known approaches) and if the time increments for explicit time-integration methods are close to the stability limit then there are no advantages in the use of the averaged mass matrix compared with the lumped mass matrix.

An interesting technique with implicit and explicit time-integration methods is suggested in [10] for acoustic waves. It is based on the modified integration rule for the calculation of the mass and stiffness matrices for linear finite elements. In contrast to the averaged mass matrix, the use of the modified integration rule increases the accuracy for the phase velocity from the second order to the fourth order in the general multi-dimensional case of acoustic waves. However, the effect of the size of time increments on the accuracy of numerical results has not been studied in [10]. The technique in [10] has not also treated spurious oscillations that may significantly destroy the accuracy of numerical results and lead to divergent results.

We should mention that the analysis of numerical dispersion estimates the numerical error for propagation of harmonic waves only. In the general case of loading (boundary conditions), the estimation of the accuracy of numerical techniques with reduced dispersion is difficult due to the presence of spurious high-frequency oscillations in numerical solutions; e.g., see [3,5].

In our previous papers [19–25], we have developed the accurate finite element techniques for elastodynamics problems. In this paper we have extended these techniques to acoustic waves. Because for wave propagation problems small time increments are necessary for accurate numerical results, explicit time-integration methods are more effective and require less computation time than implicit time-integration methods. The paper consists of a modification of the system of semidiscrete equations Eq. (2) that can be used with explicit time-integration methods and the finite elements with reduced dispersion (Section 2); the analytical study of numerical dispersion and the effect of time increments on the dispersion error for the modified integration rule, for the averaged mass matrix technique and for the standard approach with the lumped mass matrix that are used with the linear finite elements and the explicit time-integration method (Section 2); a short description and the modification of the two-stage time-integration technique with the filtering of spurious oscillations that is suggested in our previous papers [19–24] (Appendix); and 1-D and 2-D numerical examples showing the efficiency of the new two-stage time-integration technique for the simulation of acoustic waves under a suddenly applied load (Section 3).

2. Dispersion analysis

In this section, we will analyze the averaged mass matrix technique, the modified integration rule technique and the standard approach with the lumped mass matrix that are used with explicit time-integration methods. The first two techniques reduce the numerical dispersion error and the computation time compared with the standard finite element formulations for acoustic waves. In contrast to the study of the averaged mass matrix technique and the modified integration rule technique for the scalar wave equation considered in [5,10], here we will also analyze the effect of the size of time increments on the dispersion error. Similar to the paper [5], we will first modify Eq. (2) for the use of explicit time-integration methods. Let us rewrite Eq. (2) with the diagonal (lumped) mass matrix $\boldsymbol{D}$ as follows:

$$\boldsymbol{D}\dot{\boldsymbol{V}} + \boldsymbol{K}\,\boldsymbol{U} = \boldsymbol{R}, \tag{3}$$

where $\boldsymbol{V}$ is the vector of the nodal velocities (the time derivative of the nodal field variables). Relationships between the nodal field variables and their velocities can be written down as (similar to those in [5,10])

$$\boldsymbol{D}\dot{\boldsymbol{U}} = \boldsymbol{M}\,\boldsymbol{V} \quad \text{or} \quad \boldsymbol{D}\ddot{\boldsymbol{U}} = \boldsymbol{M}\,\dot{\boldsymbol{V}} \tag{4}$$

where $\boldsymbol{M}$ is the non-diagonal mass matrix calculated by the averaged mass matrix technique (see Eq. (8) below) or by the modified integration rule technique (see Eq. (9) below). Inserting Eq. (4) into Eq. (3) we will get

$$\boldsymbol{D}\ddot{\boldsymbol{U}} + \boldsymbol{M}\,\boldsymbol{D}^{-1}\,\boldsymbol{K}\,\boldsymbol{U} = \boldsymbol{M}\,\boldsymbol{D}^{-1}\,\boldsymbol{R}. \tag{5}$$

Eq. (5) differs from the standard finite element equations with the lumped mass matrix by the stiffness matrix and the load vector which are multiplied by the term $\boldsymbol{M}\,\boldsymbol{D}^{-1}$. For the time integration of Eq. (5) we will use the standard explicit central-difference method (the most popular explicit method); e.g., see [23,26,27]. Replacing the second time derivative in Eq. (5) by the corresponding finite difference approximation used in the central-difference method, we obtain

$$\boldsymbol{D}\,[\boldsymbol{U}(t+\Delta t) - 2\boldsymbol{U}(t) + \boldsymbol{U}(t-\Delta t)]/\Delta t^2 + \boldsymbol{M}\,\boldsymbol{D}^{-1}\,\boldsymbol{K}\,\boldsymbol{U}(t) = \boldsymbol{M}\,\boldsymbol{D}^{-1}\,\boldsymbol{R}(t), \tag{6}$$

where Δt is the time increment. We will use Eq. (6) for the analysis of the numerical dispersion of the finite element formulations with the averaged mass matrix and modified integration rule techniques. One of the main difficulties in the analytical study of numerical dispersion is the complicated non-linear structure of the equation for the numerical phase velocity. Therefore, in order to simplify the dispersion analysis, we will study the residual of this equation instead of the direct calculation of the numerical phase velocity.

Propagation of harmonic plane waves in an infinite medium with

$$u(\boldsymbol{x}, t) = \bar{u} exp(i\,k(\boldsymbol{n}\cdot\boldsymbol{x} \pm c_o\,t)) \tag{7}$$

is used for the dispersion analysis. Here, $\bar{u}$ is the amplitude of the acoustic waves, $\boldsymbol{x}$ is the position vector, k is the wave number, $\boldsymbol{n}$ is the unit normal to the wave front; $\boldsymbol{k} = k\,\boldsymbol{n}$ is the wave vector, c_o is the phase velocity, t is the time, and $i = \sqrt{-1}$. It can be easily checked that Eq. (7) meets Eq. (1) with $f = 0$; i.e., harmonic plane waves propagate with the constant wave velocity c_o and an isotropic infinite homogeneous medium is non-dispersive.

Below we study the numerical dispersion of linear quadrilateral finite elements on uniform meshes in the 2-D case. Because acoustic waves propagate in all directions with the same velocity, then finite elements with the same dimensions along the coordinate axes can be recommended for wave propagation problems in the multi-dimensional case (e.g., see [1,6,10] and others). They are also used in the current paper. In order to decrease the dispersion of finite element results, we consider the following two possibilities for the calculation of the mass and stiffness matrices: the mass matrix $\boldsymbol{M}$ is calculated as a weighted average of the consistent $\boldsymbol{M}^{cons}$ and lumped $\boldsymbol{D}$ mass matrices with the weighting factor γ (similar to that used in [5,6,8])

$$\boldsymbol{M}(\gamma) = \boldsymbol{D}\gamma + \boldsymbol{M}^{cons}(1-\gamma) \tag{8}$$

or the mass and stiffness matrices of each finite element are calculated with the modified integration rule (similar to those used in [10])

$$\begin{aligned}\boldsymbol{M}^e(\alpha_M) &= \int_{-1}^{1}\int_{-1}^{1}\boldsymbol{N}^T(s,t)\boldsymbol{N}(s,t)det(\boldsymbol{J})dsdt\\ &\approx \sum_{m=1}^{2}\sum_{j=1}^{2}\boldsymbol{N}^T((-1)^m\alpha_M,(-1)^j\alpha_M)\boldsymbol{N}((-1)^m\alpha_M,(-1)^j\alpha_M)det(\boldsymbol{J}),\end{aligned} \tag{9}$$

$$\begin{aligned}\boldsymbol{K}^e(\alpha_K) &= c_o^2\int_{-1}^{1}\int_{-1}^{1}\frac{\partial\boldsymbol{N}^T}{\partial\boldsymbol{x}}(s,t)\frac{\partial\boldsymbol{N}}{\partial\boldsymbol{x}}(s,t)det(\boldsymbol{J})dsdt\\ &\approx c_o^2\sum_{m=1}^{2}\sum_{j=1}^{2}\frac{\partial\boldsymbol{N}^T}{\partial\boldsymbol{x}}((-1)^m\alpha_K,(-1)^j\alpha_K)\frac{\partial\boldsymbol{N}}{\partial\boldsymbol{x}}((-1)^m\alpha_K,(-1)^j\alpha_K)det(\boldsymbol{J})\end{aligned} \tag{10}$$

in the 2-D case. Here, $\boldsymbol{N}$ is the standard finite element shape matrix; the diagonal terms of the lumped mass matrix $\boldsymbol{D}$ (except those for the boundary nodes) for the linear elements are dx^2 for square elements; $\boldsymbol{J}$ is the Jacobian matrix ($det(\boldsymbol{J}) = dx^2/4$); dx is the length of a finite element; s, t are the isoparametric coordinates; α_M and α_K are the coordinates of the integration points for the mass and stiffness matrices to be determined, respectively ($2\times 2 = 4$ integration points are used for linear elements in the 2-D case); e.g., see [26,27] for the derivation of the finite element matrices. The integration error due to the application of the modified integration rule for the mass and stiffness matrices does not change the convergence rate of finite element solutions; see [10]. We use the dispersion analysis presented below in order to find such γ, α_M and α_K that reduce the dispersion error.

Similar to Eq. (7), the numerical solution u^{num} for the propagation of harmonic plane waves in an infinite medium can be written as

$$u^{num}(\boldsymbol{x},t) = \bar{u}^{num}exp(i\,k(\boldsymbol{n}\cdot\boldsymbol{x}\pm c\,t)) \tag{11}$$

where c is the numerical wave velocity, and $\bar{u}^{num}$ is the amplitude of the acoustic waves. For the analysis of the numerical wave velocity c on a uniform mesh in the 2-D case, only one algebraic equation for any node should be used. It can be obtained by the substitution of the nodal field variables (calculated with the help of Eq. (11)) into Eq. (6). This non-linear algebraic equation $E(c) = 0$ can be determined by the consideration of four adjacent finite elements with a common node. From the solution of the equation $E(c) = 0$ we can find c. Due to the numerical dispersion error, $E(c = c_o) \neq 0$ and the deviation of $E(c = c_o)$ from zero is related to the numerical dispersion error (the decrease in $|E(c = c_o)|$ corresponds to the decrease in the dispersion error). Due to the lengthy expression for $E(c = c_o)$, we present it only for small Δt and dx (dx is the length of a square finite element) using a Taylor series

$$E(c = c_o) = \left(a_4k^4dx^4 + a_6k^6dx^6 + O\left(dx^8\right)\right), \tag{12}$$

where the expressions for coefficients a_4 and a_6 are given below for the different techniques.

2.1. The modified integration rule

In the case of the calculation of the mass and stiffness matrices with the help of Eqs. (9) and (10), the coefficients a_4 and a_6 can be found as follows:

$$\begin{aligned}a_4 &= \frac{1}{48}\{[-4\tau^2 - 3(4{\alpha_M}^2 + {\alpha_K}^2 - 6)] + [3{\alpha_K}^2 - 2]\cos(4\Theta)\},\\ a_6 &= \frac{1}{5760}\{16\tau^4 - 5[9({\alpha_M}^2 + 2{\alpha_K}^2 - 8){\alpha_M}^2 - 24{\alpha_K}^2 + 71] + 3[5(3{\alpha_M}^2 + 6{\alpha_K}^2 - 8){\alpha_M}^2 - 40{\alpha_K}^2 + 33]\cos(4\Theta)\}.\end{aligned} \tag{13}$$

Here $\tau = \frac{c_o\Delta t}{dx}$ is the Courant number, the components of the unit vector $\boldsymbol{n}$ in Eq. (7) are represented as $n_1 = \cos(\Theta)$ and $n_2 = \sin(\Theta)$. Assuming that the expressions in two square brackets for coefficient a_4 in Eq. (13) are zeros, from these two algebraic equations we can find such $\alpha_K = \sqrt{\frac{2}{3}}$ and $\alpha_M = \sqrt{\frac{4-\tau^2}{3}}$ at which $a_4 = 0$ and the dispersion error is decreased from the second order to the fourth order. The coefficient a_6 in this case is

$$a_6\left(\alpha_M = \sqrt{\frac{4-\tau^2}{3}}, \alpha_K = \sqrt{\frac{2}{3}}\right) = \frac{11\tau^4 - 60\tau^2 + (5\tau^4 - 20\tau^2 + 19)\cos(4\Theta) + 45}{5760}. \tag{14}$$

A time increment Δt for the explicit central-difference method can vary between zero and the stability limit Δt^{st}; i.e., $0 \le \Delta t \le \Delta t^{st}$. As a consequence, the range of the Courant number is $0 \le \tau \le \tau^{st} = \frac{c_o\Delta t^{st}}{dx}$. As shown in [10], $\tau^{st} = 0.7587$ for the modified integration rule technique. The analysis of Eq. (14) (see also Fig. A.1) shows that at any angle Θ, the absolute value of coefficient $a_6(\alpha_M = \sqrt{\frac{4-\tau^2}{3}}, \alpha_K = \sqrt{\frac{2}{3}})$ has the minimum value at $\tau = \tau^{st}$; i.e., the dispersion error has a minimum value at time increments close to the stability limit Δt^{st}; see also curve 2 in Fig. A.2 for a_6 at $\tau = \tau^{st}$.

2.2. The averaged mass matrix

Another way to reduce the numerical dispersion is based on the calculation of the mass matrix according to Eq. (8) and the stiffness matrix according to Eq. (10). In this case, coefficients a_4 and a_6 in Eq. (12) are as follows:

$$\begin{aligned}a_4 &= \frac{1}{48}\{[-3{\alpha_K}^2 - 4\tau^2 - 8\gamma + 14] + [3{\alpha_K}^2 - 2]\cos(4\Theta)\}\\ a_6 &= \frac{(45 - 30\gamma){\alpha_K}^2 + 4(2\tau^4 + 25\gamma - 30) + (15(2\gamma - 3){\alpha_K}^2 - 20\gamma + 32)\cos(4\Theta)}{2880}.\end{aligned} \tag{15}$$

Assuming that the expressions in two square brackets for coefficient a_4 in Eq. (15) are zeros, from these two algebraic equations we can find such $\alpha_K = \sqrt{\frac{2}{3}}$ and $\gamma = \frac{3-\tau^2}{2}$ at which $a_4 = 0$ and the dispersion error decreases from the second order to the fourth order. The coefficient a_6 in this case is

$$a_6\left(\gamma = \frac{3-\tau^2}{2}, \alpha_K = \sqrt{\frac{2}{3}}\right) = \frac{15 - 20\tau^2 + \tau^4 + \cos(4\Theta)}{1440}. \tag{16}$$

As shown in [10], $\tau^{st} = 0.805$ in this case. The analysis of Eq. (16) (see also Fig. A.3) shows that at any angle Θ, the absolute value of coefficient $a_6(\gamma = \frac{3-\tau^2}{2}, \alpha_K = \sqrt{\frac{2}{3}})$ has the minimum value at $\tau = \tau^{st}$; i.e., the dispersion error has a minimum value at time increments close to the stability limit Δt^{st}; see also curve 1 in Fig. A.2 for a_6 at $\tau = \tau^{st}$. From Figs. A.1 and A.3 we can also see that the maximum dispersion error (or the maximum absolute value of coefficient a_6) in the 2-D case occurs for the acoustic waves propagating along the Cartesian axes with $\Theta = 0, \frac{\pi}{2}$ for the two cases considered above; at $\tau = \tau^{st}$ for each technique, this error is slightly smaller for the technique with $\gamma = \frac{3-\tau^2}{2}$ and $\alpha_K = \sqrt{\frac{2}{3}}$; see curves 1 and 2 in Fig. A.2. Therefore, for the numerical examples in Section 3 we will consider the technique with reduced dispersion based on $\gamma = \frac{3-\tau^2}{2}$ and $\alpha_K = \sqrt{\frac{2}{3}}$ (this technique also allows slightly larger time increments compared with those for the technique based on $\alpha_M = \sqrt{\frac{4-\tau^2}{3}}$ and $\alpha_K = \sqrt{\frac{2}{3}}$ as indicated above).

The dispersion error for the approaches based on the averaged mass matrix and the standard stiffness matrix (e.g., see [5]) can also be obtained from Eq. (15). For the standard stiffness matrix, the location of the integration points corresponds to $\alpha_K = \sqrt{\frac{1}{3}}$. In this case, coefficients a_4 and a_6 in Eq. (15) are

$$a_4\left(\gamma = \frac{3-\tau^2}{2}, \alpha_K = \sqrt{\frac{1}{3}}\right) = \frac{1}{24}\sin^2(2\Theta),$$

$$a_6\left(\gamma = \frac{3-\tau^2}{2}, \alpha_K = \sqrt{\frac{1}{3}}\right) = \frac{30 - 45\tau^2 + 8\tau^4 + (2 + 5\tau^2)\cos(4\Theta)}{2880}. \tag{17}$$

As can be seen, for the standard stiffness matrix, the coefficient a_4 in Eq. (17) is independent of the Courant number τ and equals zero at the angles $\Theta = 0, \frac{\pi}{2}, \pi, \frac{3\pi}{2}$ in the range $0 \le \Theta \le 2\pi$ (for all other angles the coefficient $a_4 \ne 0$); see Fig. A.4. For example, at $\Theta = 0, \frac{\pi}{2}, \pi, \frac{3\pi}{2}$, the coefficient a_4 is zero and the absolute value of the coefficient a_6 in Eq. (17) has the minimum value at $\tau = \tau^{st}$. Therefore, in the case of the averaged mass matrix and the standard stiffness matrix, time increments close to the stability limit can be recommended for the decrease in the dispersion error. It can be checked that the stability limit in this case corresponds to $\tau^{st} = 1$; i.e., $\gamma = \frac{3-\tau^2}{2} = 1$ at $\tau = \tau^{st} = 1$ and according to Eq. (8), this case reduces to the standard approach with the lumped mass matrix and the time increments equal to the stability limit.

It is also necessary to note that the weighting coefficient $\gamma = 1.5$ was used in the average mass technique suggested in [5]. However, as can be seen from Eq. (15), $\gamma = 1.5$ does not lead to the decrease in the order of the dispersion error at finite time increments even in the 1-D case (i.e., the coefficient a_4 is non-zero); see also the numerical example below. Only for very small time increments $\Delta t \approx 0$ (or $\tau \approx 0$), the weighting coefficient derived above from Eq. (15) is $\gamma = \frac{3-\tau^2}{2} \approx 1.5$.

2.3. The standard approach with the lumped mass matrix

For the standard approach with the lumped mass matrix ($\gamma = 1$) and the standard stiffness matrix ($\alpha_K = \sqrt{\frac{1}{3}}$), the dispersion error can also be analyzed with the help of Eq. (15). The coefficient a_4 in this case is

$$a_4\left(\gamma = 1, \alpha_K = \sqrt{\frac{1}{3}}\right) = \frac{1}{48}(-4\tau^2 - \cos(4\Theta) + 5). \tag{18}$$

According to Eq. (18), the coefficient a_4 has the minimum value at $\tau = \tau^{st} = 1$ for all angles Θ; see Fig. A.5 (as we mentioned in the previous Section 2.2, the stability limit is $\tau^{st} = 1$ for the standard approach). That is, $a_4(\gamma = 1, \alpha_K = \sqrt{\frac{1}{3}}) = \frac{1}{24}\sin^2(2\Theta)$ at $\tau = \tau^{st} = 1$.

Remark. The dispersion error in the 1-D case for all approaches considered above coincides with that from the formulas for the 2-D case at $\Theta = 0$. It can be shown that all coefficients in a Taylor series of $E(c = c_o)$ are zero in the 1-D case at $\tau = \tau^{st} = 1$; i.e., in this case the dispersion error is zero. In contrast to the 1-D case, the dispersion error in the 2-D case for $\tau = \tau^{st} = 1$ is zero only for the waves propagating along the Cartesian axes ($\Theta = 0, \frac{\pi}{2}$) and has the maximum value for the waves propagating along the directions at which $\sin^2(2\Theta) = 1$ (or at $\Theta = \frac{\pi n}{4}$ where $n = 1, 3, 5, \ldots$); see also Fig. A.4. In this case the coefficient a_4 is $a_4 = \frac{1}{24}$ at $\Theta = \frac{\pi n}{4}$ and $\tau = \tau^{st} = 1$. It is interesting to note that for the same dispersion error in the 1-D case ($\Theta = 0$), the Courant number should be $\tau \approx 0.71$; i.e., $a_4(\gamma = 1, \alpha_K = \sqrt{\frac{1}{3}}) \approx \frac{1}{24}$ at $\Theta = 0$ and $\tau \approx 0.71$. We will use this $\tau \approx 0.71$ for the determination of coefficients a_1 and a_2 in Eqs. (A.1)–(A.3) used for the standard approach at the filtering stage ; see the Appendix.

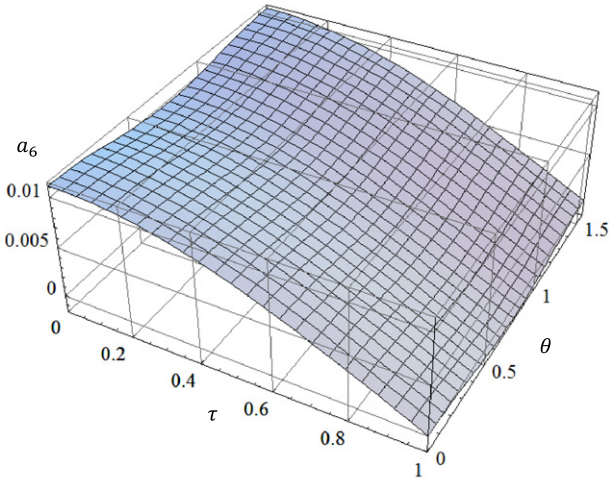

Fig. A.1. Coefficient a_6 in Eq. (14) as a function of Θ and τ.

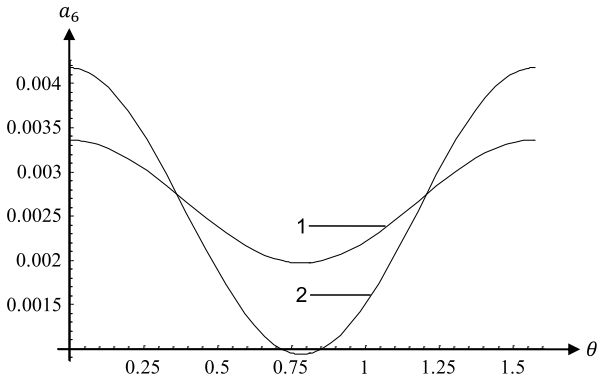

Fig. A.2. Coefficients a_6 in Eq. (16) at $\tau = \tau^{st} = 0.805$ (curve 1) and in Eq. (14) at $\tau = \tau^{st} = 0.7587$ (curve 2) as a function of Θ.

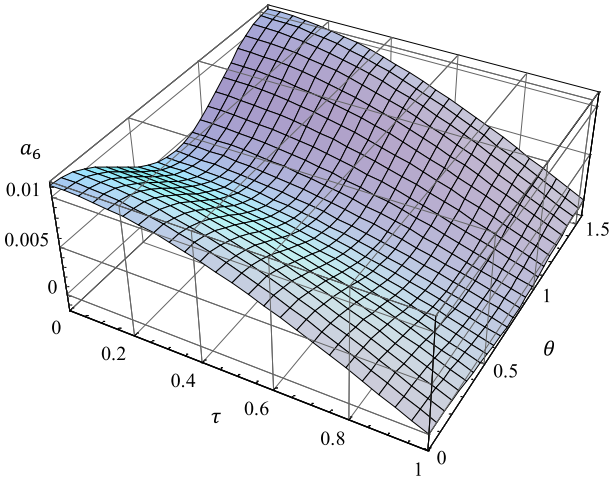

Fig. A.3. Coefficient a_6 in Eq. (16) as a function of Θ and τ.

3. Numerical modeling

The finite element approaches for acoustic problems based on the reduced dispersion technique and on the standard technique with the lumped mass matrix are implemented into the finite element code FEAP [28]. Below they are used for 1-D and 2-D acoustic wave propagation problems under a suddenly applied load for which all low and high frequencies are excited. Due to spurious high-frequency oscillations, these problems cannot be accurately solved by existing time-integration methods based on the introduction of artificial viscosity (or numerical dissipation) at each time increment, especially in the case of long-term integration. Therefore, the two-stage time-integration technique developed in our previous papers [21–23] (see also the Appendix) is used. The filtering stage of this technique includes the time continuous Galerkin (TCG) method with $N = 10$ time increments (5 positive plus 5 negative time increments) the size of which is calculated according to Eqs. (A.1)–(A.3) (see [21–23] and the Appendix below).

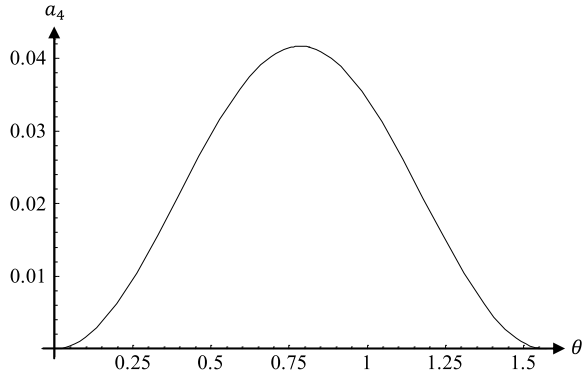

Fig. A.4. Coefficient a_4 in Eq. (17) as a function of Θ.

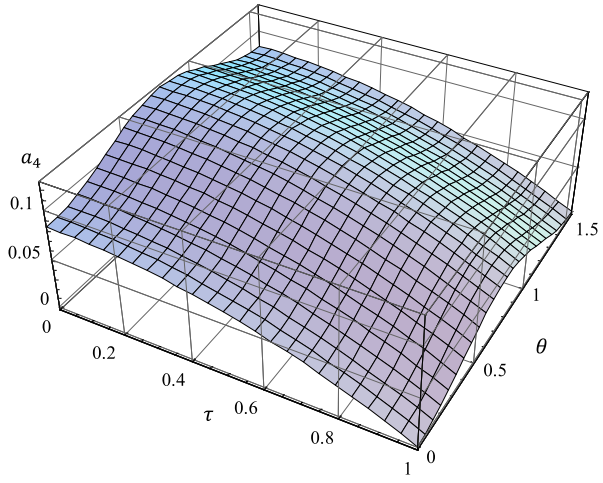

Fig. A.5. Coefficient a_4 in Eq. (18) as a function of Θ and τ.

3.1. 1-D elastic bar under a suddenly applied load

First, an elastic bar of the length $L = 4$ under a suddenly applied load is considered in the 1-D case (see Fig. A.6(a)). The wave velocity is chosen to be $c_o = 1$. The following boundary conditions are applied: $u(0, t) = t$ (which corresponds to the velocity $v(0, t) = v_0 = 1$) and $u(4, t) = 0$ (which corresponds to the velocity $v(4, t) = 0$). Zero initial conditions are used; i.e., $u(x, 0) = v(x, 0) = 0$. The observation time is chosen to be $T = 18$. During this time the waves travel within the bar with two reflections from each end of the bar. The analytical solution to this problem for the velocity at $T = 18$ is: $v_a(x, 18) = 1$ for $0 \le x < 2$ and $v_a(x, 18) = 0$ for $2 < x \le 4$ (at $x = 2$, a jump in the velocity occurs).

It is known that the application of traditional semi-discrete methods to this problem leads to oscillations in velocities due to the spurious high-frequency response [20,23,29]. The finite elements with reduced numerical dispersion reduce these oscillations after basic computations but they do not remove them from the numerical solution (e.g., see Fig. A.6(b)). Therefore, the two-stage procedure with the basic computations and the filtering stage as described in the Appendix is applied for accurate and non-oscillatory solutions.

The problem is solved on a uniform mesh with 100 linear two-node finite elements and the averaged mass matrices with $\gamma = \frac{3-\tau^2}{2}$ as described in Section 2.2 and with $\gamma = 1.5$ as suggested in [5]. The standard explicit central-difference method in time based on Eq. (5) is applied (for the lumped mass matrix $\boldsymbol{M} = \boldsymbol{D}$, Eq. (5) reduces to the standard form of the explicit central-difference method). We should mention that the techniques based on the modified integration rule with $\alpha_M = \sqrt{\frac{4-\tau^2}{3}}$ and on the averaged mass matrix with $\gamma = \frac{3-\tau^2}{2}$ are completely equivalent and yield the same results in the 1-D case; see [25]. For $\Delta t = \Delta t^{st}$ (or $\tau = 1$), these techniques coincide with the standard approach with the lumped mass matrix and yield the analytical solution. In basic computations, we use the time increments $\Delta t_1 = 0.03197$ corresponding to the Courant number $\tau \approx 0.8$ as well as the very small time increments $\Delta t_2 = \Delta t_1/20 = 0.001599$ (much smaller than the stability limit $\Delta t^{st} = 0.04$). For the filtering stage, we use the time increments $\Delta t_1' = 0.03245$, $\Delta t_2' = 0.0405$ and $\Delta t_1'' = 0.06747$ for the results obtained in basic computations with $\gamma = \frac{3-\tau^2}{2}$ and $\Delta t_1 = 0.03197$, with $\gamma = \frac{3-\tau^2}{2}$ and $\Delta t_2 = 0.001599$, with $\gamma = 1.5$ and $\Delta t_1 = 0.03197$, respectively. The time increments at the filtering stage have been determined from numerical experiments and correspond to the same small amplitudes of spurious oscillations (with the relative error of 0.5%); see our papers [21,23].

The velocity distribution and the corresponding error in velocity $e = v_{numer} - v_{exact}$ at time $T = 18$ are shown in Fig. A.6 after basic computations (b, d) and after the filtering stage (c, e). After basic computations, all numerical results include spurious oscillations (compare curves 2–4 in Fig. A.6(b) with the analytical solution, curve 1) and it is difficult to compare their accuracy. After the filtering of spurious oscillations we can see in Fig. A.6(c) that for the average mass matrix technique ($\gamma = \frac{3-\tau^2}{2}$), the time increments $\Delta t_1 = 0.03197$ ($\tau \approx 0.8$) in basic computations yield slightly more accurate solutions than very small time increments $\Delta t_2 = \Delta t_1/20 = 0.001599$; see curves 2 and 3. This is also in agreement with the dispersion analysis; see Section 2. However, at the same finite time increments $\Delta t_1 = 0.03197$

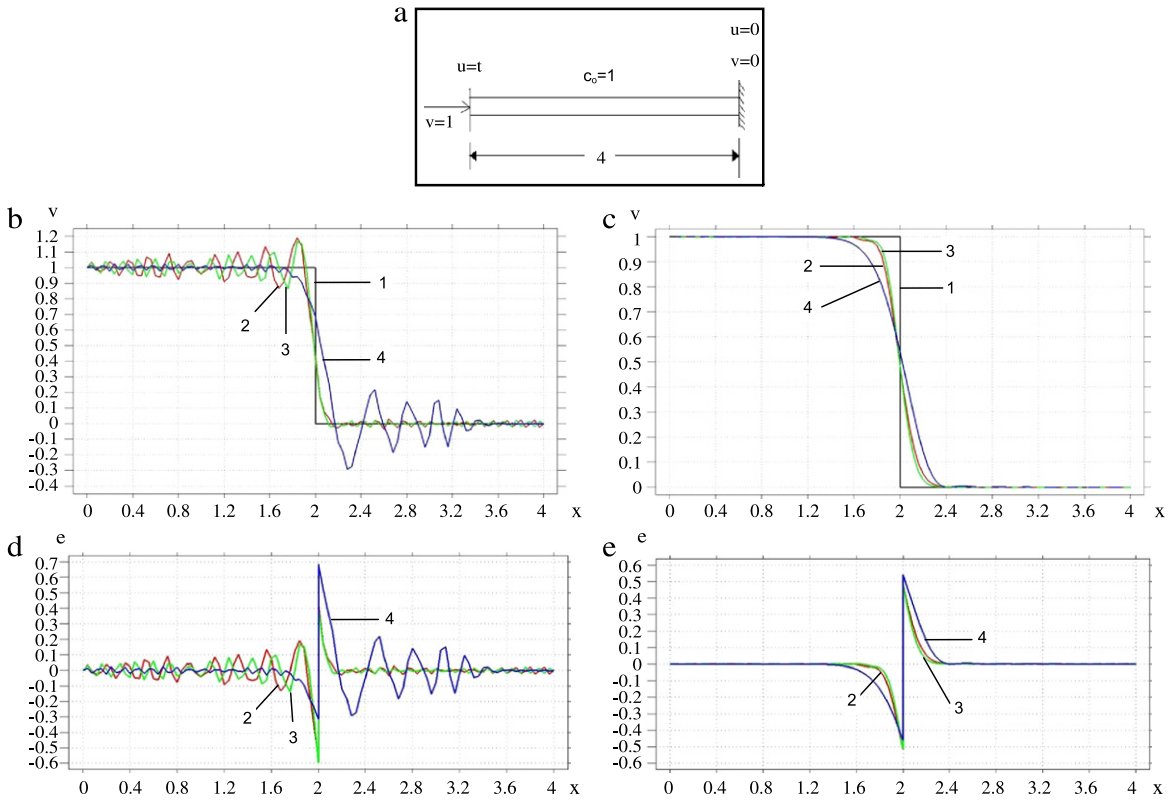

Fig. A.6. An elastic bar of length $L = 4$ under a suddenly applied load (a). The velocity distribution (b, c) and the corresponding error (d, e) along the bar and at the observation time $T = 18$ after basic computations (b, d) and after the filtering stage (c, e). Curves 1 correspond to the analytical solution. Curves 2 and 3 correspond to the average mass matrix with $\gamma = \frac{3-\tau^2}{2}$ and the time increments $\Delta t_2 = 0.001599$ and $\Delta t_1 = 0.03197$ in basic computations, respectively. Curves 4 correspond to the average mass matrix with $\gamma = 1.5$ (as in [5]) and the time increments $\Delta t_1 = 0.03197$ in basic computations.

in basic computations, the averaged mass matrix with $\gamma = \frac{3-\tau^2}{2}$ yields much more accurate results than that with $\gamma = 1.5$ as suggested in [5]; compare curves 3 and 4 in Fig. A.6(c); i.e., the technique suggested in [5] does not yield any advantage compared with the standard approach at time increments comparable with the stability limit; see also Section 2.2.

3.2. 2-D plate under a suddenly applied concentrated load

Let us consider a square plate of length 2×2 instantly loaded in the center. Due to symmetry, Fig. A.7(a) includes only a quarter of the plate where the x- and y-axes are the axes of symmetry and $AD = AB = 1$. The wave velocity is chosen to be $c_o = 1$. The following boundary conditions are applied: $\frac{\partial u}{\partial n} = 0$ along the entire boundary AB, BC, CD and AD ($\frac{\partial}{\partial n}$ is the normal derivative at the boundary); a concentrated load is instantly applied at point A and is prescribed in terms of the value of the function $u(0, 0, t) = 1$. Zero initial conditions are used; i.e., $u(x, y, 0) = v(x, y, 0) = 0$. The observation time is chosen to be $T = 0.8$. During this time the waves travel from point A to the boundary but do not reach it. Therefore, the zero boundary conditions at BC and CD do not affect the solution at time $T = 0.8$. By symmetry, the solution to this problem at any point depends on the radius with the center at point A and is independent of the angle between the radius and the x-axis.

The problem is solved on uniform meshes with $100 \times 100 = 10\,000$, $300 \times 300 = 90\,000$, and $800 \times 800 = 640\,000$ linear four-node quadrilateral finite elements by the reduced dispersion technique with ($\gamma = \frac{3-\tau^2}{2}$ and $\alpha_K = \sqrt{\frac{2}{3}}$) as well as by the standard approach with the lumped mass matrix. The time increments close to the stability limit are used in basic computations; i.e., the time increments corresponding to $\tau = 0.8$ for the reduced dispersion technique and $\tau = 1$ for the standard approach with the lumped mass matrix. For the filtering stage, the time increments are defined by Eqs. (A.1)–(A.3) from the Appendix; see also the corresponding explanations in the Appendix.

Fig. A.7 shows the distribution of the field variable and its time derivative at the observation time $T = 0.8$ after basic computations and after the filtering stage obtained on a uniform mesh with $100 \times 100 = 10\,000$ linear four-node quadrilateral finite elements by the reduced dispersion technique. As can be seen from Fig. A.7, the filtering stage (c) just slightly improves the numerical anisotropy of the field variable u after basic computations (b) for which the small oscillations of isolines can be seen. However, due to large spurious oscillations, the numerical anisotropy of the velocity v after basic computations (see (d)) is very large and makes the results non-valid (the exact solution corresponds to circular isolines for the problem). However, the filtering stage significantly reduces the numerical anisotropy for the velocity; see (e).

Let us consider the error for the velocity in Fig. A.7 in more detail by plotting the velocity along the x-axis (line AD in Fig. A.7(a)) and along the line forming angle $\Theta = \pi/4$ with the x-axis (line AC in Fig. A.7(a)); see Fig. A.8. The amplitudes of spurious oscillations after basic computations are different at different directions; see curves 1 and 2 in Fig. A.8(a). After the filtering stage, the solution for the velocity is totally different from that in basic computations; see curves 1 and 2 in Fig. A.8(b). The curves 1 and 2 after the filtering stage almost coincide; i.e., the filtering of spurious oscillations significantly reduces the numerical anisotropy.

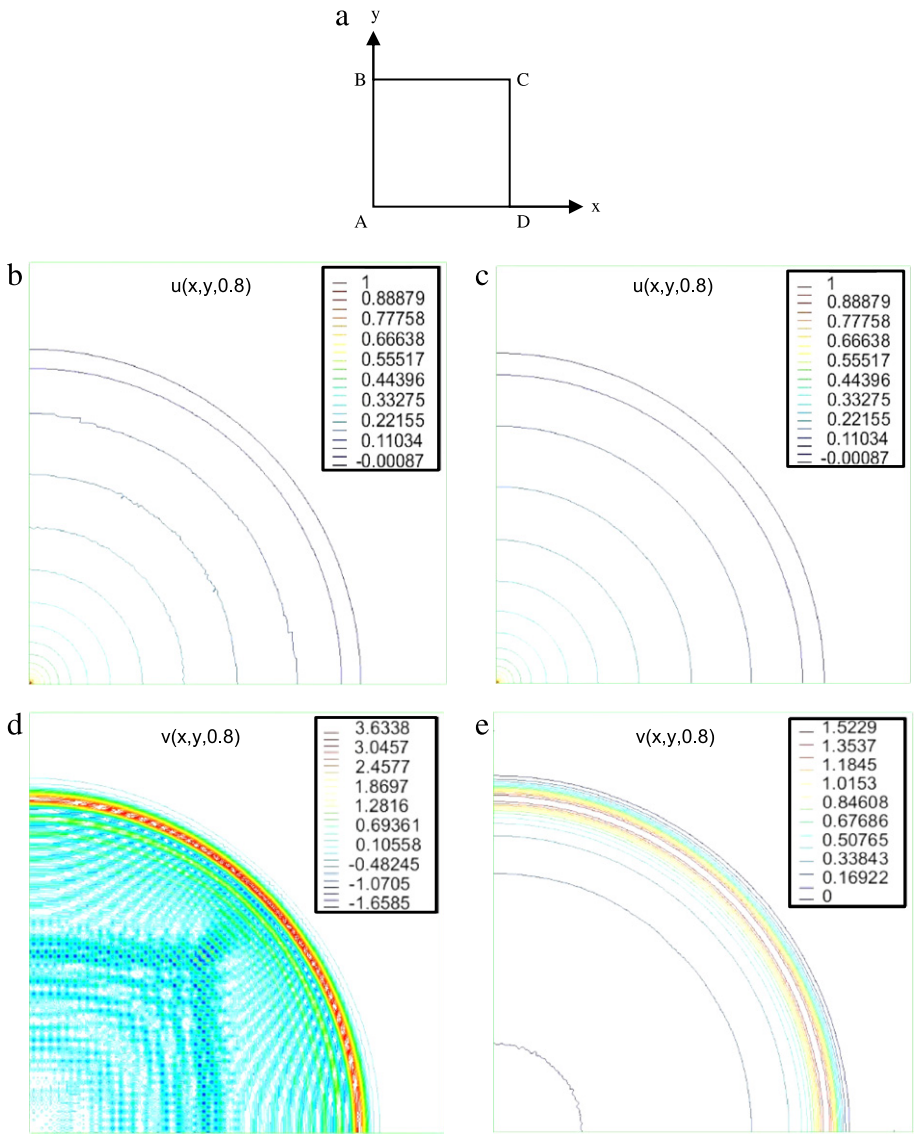

Fig. A.7. 2-D plate under a suddenly applied concentrated load (a). The distribution of the field variable $u(x, y, 0.8)$ (b, c) and its time derivative $v(x, y, 0.8)$ (d, c) at the observation time $T = 0.8$ after basic computations (b, d) and after the filtering stage (c, e). A uniform mesh with $100 \times 100 = 10\,000$ linear four-node quadrilateral finite elements and the reduced dispersion technique with $\gamma = \frac{3-\tau^2}{2}$ and $\alpha_K = \sqrt{\frac{2}{3}}$ are used.

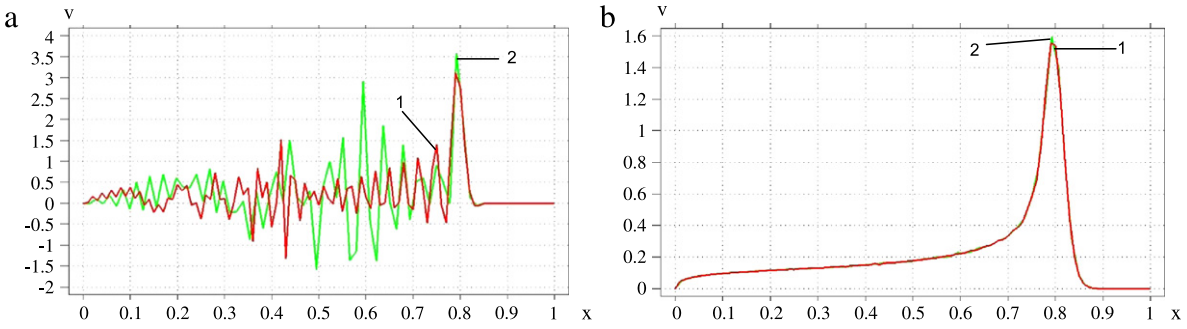

Fig. A.8. The velocity distribution along AD (curves 1) and along AC (curves 2) at the observation time $T = 0.8$ after basic computations (a) and after the filtering stage (b); see Fig. A.7(a) for AD and AC. A uniform mesh with $100 \times 100 = 10\,000$ linear four-node quadrilateral finite elements and the reduced dispersion technique with $\gamma = \frac{3-\tau^2}{2}$ and $\alpha_K = \sqrt{\frac{2}{3}}$ are used.

It is interesting to note that mesh refinement without the filtering stage does not improve the numerical solutions. Moreover, we have divergent results at mesh refinement due to the increase in the amplitudes of spurious oscillations; see Fig. A.9(a)–(c). However, the two-stage time-integration approach with the filtering stage yields convergent results at mesh refinement; see Fig. A.9(d).

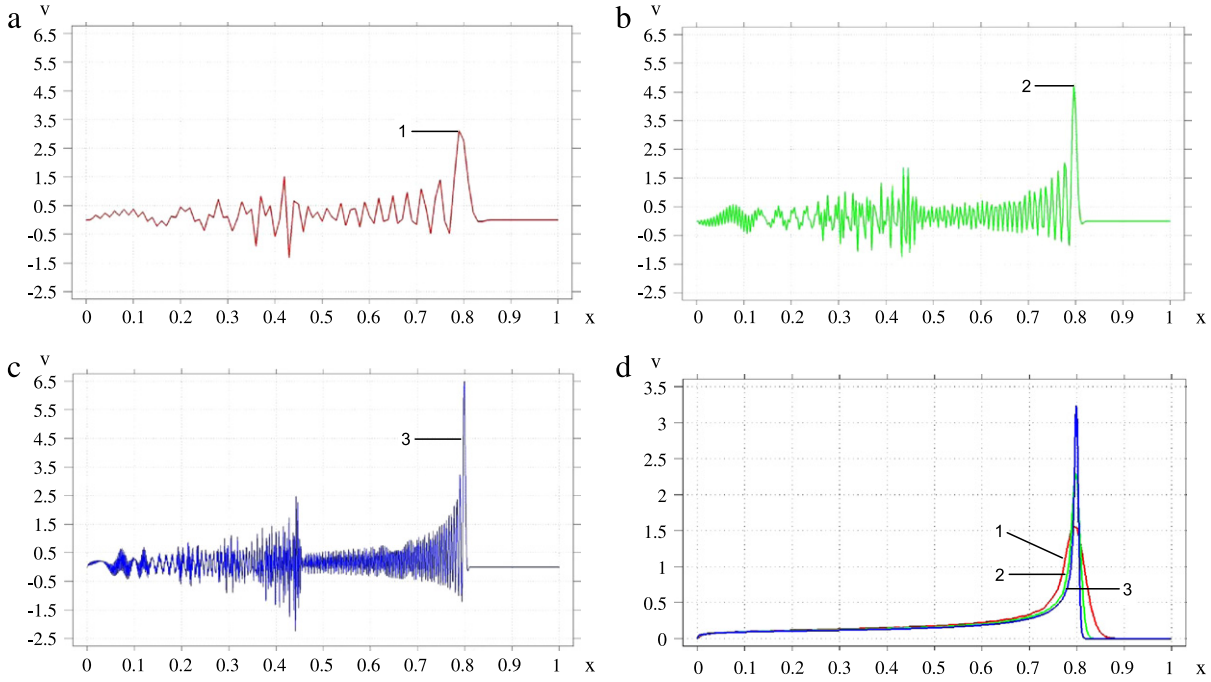

Fig. A.9. The velocity distribution along AD at the observation time $T = 0.8$ after basic computations (a, b, c) and after the filtering stage (d). Curves 1, 2 and 3 correspond to the uniform meshes with $100 \times 100 = 10\,000$, $300 \times 300 = 90\,000$, and $800 \times 800 = 640\,000$ linear four-node quadrilateral finite elements and the use of the reduced dispersion technique with $\gamma = \frac{3-\tau^2}{2}$ and $\alpha_K = \sqrt{\frac{2}{3}}$.

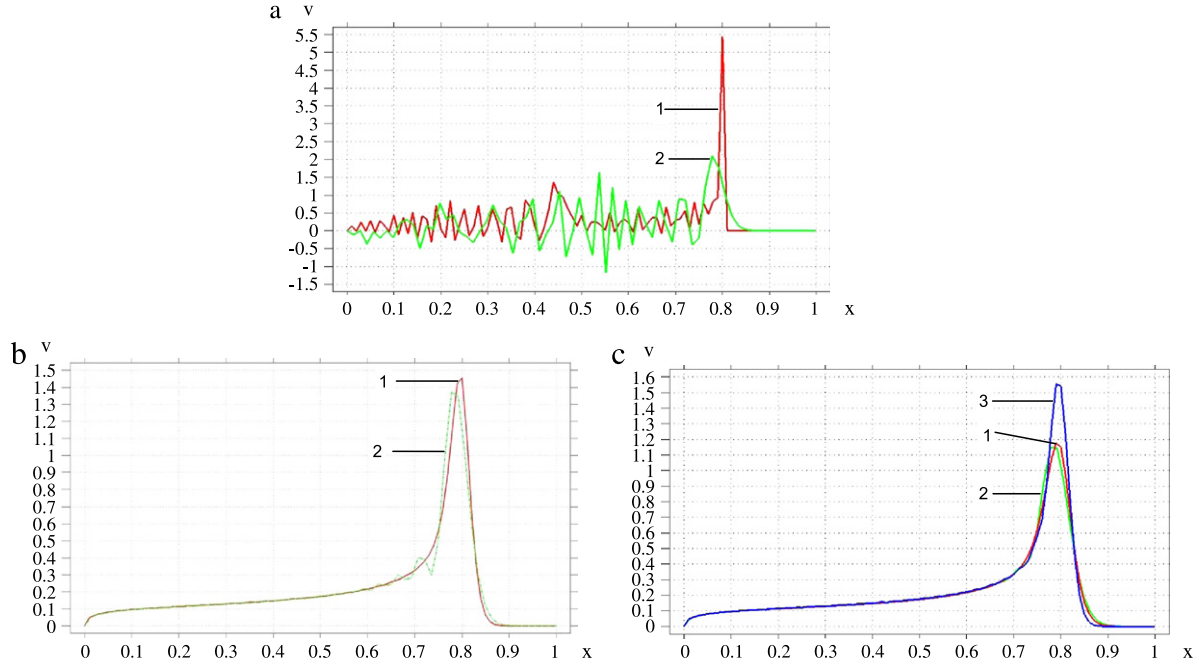

Fig. A.10. The velocity distribution along AD (curves 1) and along AC (curves 2) at the observation time $T = 0.8$ after basic computations (a) and after the filtering stage (b, c); see the text for explanations. A uniform mesh with $100 \times 100 = 10\,000$ linear four-node quadrilateral finite elements, the standard approach with the lumped mass matrix and the time increments equal to the stability limit in basic computations are used. The range of frequencies filtered in (b) is the same as that in Fig. A.8(b) for the reduced dispersion technique. Curve 3 in (c) corresponds to curve 1 in Fig. A.8(b).

As we mentioned in Section 2.3, the standard approach with the lumped mass matrix and the time increments equal to the stability limit yields the analytical solution in the 1-D case. Therefore, it is interesting to study the accuracy of the standard approach at the time increments equal to the stability limit in the 2-D case. As can be seen from Fig. A.10(a), for the standard approach the velocity distributions after basic computations along lines AD ($\theta = 0$) and AC ($\theta = \pi/4$) are very different and the velocity distribution is more accurate along AD as predicted by the dispersion analysis in Section 2.3. If for the filtering stage we use the same time increments as those for the reduced dispersion technique in Figs. A.7–A.9 (i.e., we use the same coefficients a_1 and a_2 in Eqs. (A.1)–(A.3)), then the velocity along line AD does not have spurious oscillations (see curve 1 in Fig. A.10(b)) and is close to that in Fig. A.8(b); however, the velocity along line AC still has several spurious oscillations (see curve 2 in Fig. A.10(b)). Therefore, in order to remove spurious oscillations in all directions, we

will use the coefficients a_1 and a_2 in Eqs. (A.1)–(A.3) from the Appendix determined in the 1-D case for the standard approach with the time increments corresponding to $\tau \approx 0.71$ (see Section 2.3 and the Appendix). In this case, spurious oscillations have been removed from the numerical results (see curves 1 and 2 in Fig. A.10(c)). A small difference between curves 1 and 2 in Fig. A.10(c) corresponds to the numerical anisotropy of the standard approach. We can also see that the reduced dispersion technique yields much more accurate results than the standard approach (see curves 1 and 3 in Fig. A.10(c)).

4. Concluding remarks

The paper considers accurate finite element solutions for the propagation of acoustic waves based on the application of the two-stage time-integration approach with the explicit central-difference time-integration method in basic computations. For the space discretization, we use the standard linear finite elements as well as the linear elements with reduced dispersion. However, any other space-discretization techniques such as the spectral elements, the isogeometric elements, the boundary element method, different meshless methods and many others can be applied with the approach suggested in the paper. The new findings of the paper can be summarized as follows.

- In contrast to the results in [10], we use the dispersion analysis of the reduced dispersion technique and the standard finite element approach for transient acoustic problems in order to determine the effect of the size of time increments on the dispersion error. We have found that the decrease in the size of time increments leads to the increase in the dispersion error for both techniques. Therefore, the time increments close to the stability limit in basic computations yield the most accurate numerical solutions. We should mention that these results are totally different from those for multi-dimensional elastodynamics problems for which smaller time increments in basic computations yield more accurate solutions for the linear elements with reduced dispersion; see [25].
- We have shown that for a suddenly applied load even the reduced dispersion technique with the time increments close to the stability limit leads to divergent results at mesh refinement; e.g., see Fig. A.9(a)–(c). This is explained by the increase in the amplitudes of spurious oscillations at mesh refinement. Therefore, in order to get convergent results, for the first time we have modified and applied the two-stage time-integration technique (suggested in our papers [20,21,23] for elastodynamics) to acoustic problems. This technique allows the quantification of the range of spurious oscillations (in terms of the coefficients a_1 and a_2; see the Appendix) and their filtering from numerical solutions for different space-discretization methods at the filtering stage. For the standard approach with the lumped mass matrix, we have also used the results of the dispersion analysis of Section 2.3 for the accurate determination of the coefficients a_1 and a_2. For the first time we have shown that the application of the two-stage time-integration approach yields accurate convergent results at mesh refinement; e.g., see Fig. A.9(d). It is also interesting to note that along with the damping of spurious oscillations, the filtering stage significantly reduces the numerical anisotropy of solutions; e.g., see Figs. A.8 and A.10.
- In [10], the reduced dispersion technique and the standard technique with the lumped mass matrix are compared at the same time increments (corresponding to the Courant number $\tau = 0.75$) which are close to the stability limit for the reduced dispersion technique but are smaller than the stability limit for the standard approach ($\tau = 1$). Therefore, this comparison cannot be considered as the illustration of the advantage of the reduced dispersion technique because the time increments close to the stability limit (for $\tau = 1$) significantly improve the accuracy of the standard approach. In our paper we compare these techniques for the time increments close to the stability limit for each technique. It is interesting to note that along the Cartesian axes (as considered in [10]), the reduced dispersion technique and the standard technique yield approximately the same accuracy; e.g., see curves 1 in Figs. A.8(b) and A.10(b). However, the numerical solution for the standard technique is inaccurate in other directions as predicted by the dispersion analysis in Section 2.3 and as shown by the numerical results; e.g., see curves 2 in Fig. A.10(b). After the filtering of spurious oscillations in all directions, we show that the reduced dispersion technique is much more accurate than the standard approach; see Fig. A.10(c).

In the paper, the two-stage time-integration technique has been modified and applied to acoustic problems under a suddenly applied load. However, the filtering stage of this approach is independent of the boundary and initial conditions and can be applied to any loading with the same coefficients a_1 and a_2 at the filtering stage as described in the Appendix. Because, it is difficult to predict the amplitudes of spurious oscillations in terms of the applied loading, the filtering stage can be recommended for all acoustic problems; e.g., see our papers [20,21,23]. We should also note that this approach can be used with any space-discretization methods as well as with explicit and implicit time-integration methods, e.g., [20,21,23]. The application of the two-stage time-integration technique to wave propagation in composite materials is considered in our recent paper [30]. In this case, the exact solutions to 1-D wave propagation problems in composite materials derived in the paper [31] can be used for the accuracy estimation of numerical techniques.

Acknowledgments

The research has been supported in part by the Air Force Office of Scientific Research (contract FA9550-12-1-0324) and by Texas Tech University.

Appendix. The two-stage time-integration technique with filtering spurious oscillations (see [20,21,23])

In order to filter spurious high-frequency oscillations, numerical dissipation (or artificial damping) is usually introduced for the time integration of Eq. (2). As we showed in our paper [23], the use of a time-integration method with numerical dissipation (or artificial damping) at each time increment leads to inaccurate numerical results for low frequencies as well, especially for a long-term integration. It is also unclear how in this case to select the amount of numerical dissipation and the range of high frequencies to be filtered.

To resolve these issues, we have developed the two-stage time-integration technique (see [20,21,23]) with the stage of basic computations and the filtering stage. This technique is based on the fact that for linear elastodynamics and acoustic problems, there is no necessity to filter spurious oscillations at each time increment because the errors in high frequencies do not affect the accuracy of low frequencies during time integration; see [23]. In the current paper, we use the standard explicit central-difference time-integration method (without

numerical dissipation or artificial viscosity) in basic computations in order to obtain an accurate solution of the semi-discrete elastodynamics and acoustic problem, Eq. (2) (this solution contains spurious high-frequency oscillations). We should mention that other known explicit time-integration methods can also be used for basic computations (however, in this case the dispersion analysis of Section 2 should be modified for the corresponding explicit time-integration method). For the filtering of spurious oscillations, the implicit TCG method with large numerical dissipation developed in [23] is used at the filtering stage. For all elastodynamics and acoustic problems, we use $N = 10$ uniform time increments (5 positive plus 5 negative time increments) at the filtering stage. This means that there is no real time integration at the filtering stage (the sum of 10 time increments used at the filtering stage is zero). As shown in [23], this procedure is equivalent to the multiplication of each velocity and displacement of the uncoupled system of the semi-discrete equations by a factor of $\left(\frac{(3+m)^2+\Omega^2}{(3+m)^2+(2+m)^2\Omega^2}\right)^5$ (where $\Omega = \omega_j \Delta t$ and ω_j are the eigen-frequencies of the semi-discrete system, Δt is the time increment as well as $m = 15$ is used) and does not require the modal decomposition and the calculation of eigen-frequencies. As can be seen, this factor is close to zero for large Ω and is close to unity for small Ω. The size Δt of time increments at the filtering stage indirectly defines the amount of numerical dissipation and the range of spurious oscillations to be filtered and is calculated according to the following formulas:

$$\Delta t = \alpha\left(\frac{c_o T}{dx}\right)\frac{dx\Omega_{0.1}(N)}{c_o}, \tag{A.1}$$

with

$$\alpha\left(\frac{c_o T}{dx}\right) = a_1\left(\frac{c_o T}{dx}\right)^{a_2} \tag{A.2}$$

in the 1-D case and

$$\Delta t = \max_j\left[\alpha\left(\frac{c_o T}{dx_j}\right)\frac{dx_j}{c_o}\right]\Omega_{0.1}(N) = \max_j\left[\frac{dx_j}{c_o}\right]^{1-a_2} a_1 T^{a_2}\,\Omega_{0.1}(N) = \left[\frac{dx_{max}}{c_o}\right]^{1-a_2} a_1 T^{a_2}\,\Omega_{0.1}(N), \tag{A.3}$$

in the 2-D and 3-D cases (see our papers [21,23]). Here, c_o is the wave velocity; dx is the size of a finite element in the 1-D case; T is the observation time; $dx_{max} = \max_j dx_j$ is the maximum dimension of finite elements along the axes x_j ($j = 1, 2$ for 2-D problems and $j = 1, 2, 3$ for 3-D problems); $\Omega_{0.1}(N = 10) = 0.81$ for the TCG method with $N = 10$ time increments. Eq. (A.3) is based on Eqs. (A.1) and (A.2) with the selection of the maximum size of a time increment with respect to the maximum size of a finite element along the coordinate axes. In contrast to the 2-D and 3-D elastodynamics problems with the compressional and shear waves propagating with different wave velocities and considered in [21,23], acoustic waves propagate with the same velocity c_o in the multi-dimensional case. This simplifies Eq. (A.3) compared with that in [21,23].

Using the calibration procedure described in [21], we determined the following coefficients a_1 and a_2 for the linear elements: $a_1 = 0.3296$ and $a_2 = 0.218$ for the averaged ($\gamma = \frac{3-\tau^2}{2}$) mass matrix (or the modified integration rule) and very small time increments in basic computations; $a_1 = 0.2639$ and $a_2 = 0.3373$ for the standard approach with the lumped mass matrix and the time increments corresponding to $\tau \approx 0.71$ in basic computations (see Section 2.3). These coefficients a_1 and a_2 are calibrated in the 1-D case for the filtering of the numerical results obtained in basic computations of the 1-D impact problem and they can be used for all elastodynamics and acoustic problems; see [23]. We should mention that the coefficients a_1 and a_2 for the reduced dispersion technique with very small time increments in basic computations ($\tau \approx 0$) correspond to the worst scenario with the largest spurious oscillations. Therefore, they can be used for the numerical results obtained with any size of time increments in basic computations (the increase in time increments in basic computations improves the accuracy of the numerical results; see Section 2). For more accurate results for the standard technique, we have determined a_1 and a_2 for the standard approach with the lumped mass matrix and the time increments corresponding to $\tau \approx 0.71$ in basic computations for the 1-D case; these coefficients can be used for the multi-dimensional acoustic solutions obtained in basic computations by the standard approach with the time increments close to the stability limit $\tau \approx 1$. If very small time increments are used for the standard technique in basic computations then the following coefficients should be used: $a_1 = 0.3342$ and $a_2 = 0.3363$ (we have not used these coefficients for the numerical results presented in the paper).

We should also mention that the filtering stage can be applied in the beginning of calculations as a pre-processor, in the end of calculations as a post-processor or at some intermediate time (see [19,22–24] for numerous examples of the application of the two-stage time-integration technique).

Remark. It is interesting to note that in contrast to acoustic problems, smaller time increments in basic computations of elastodynamics problems yield more accurate results for the reduced dispersion techniques in the multi-dimensional case; see [25].

References

[1] H.P. Cherukuri, Comput. Mech. 25 (2000) 317–328.
[2] W. Dauksher, A.F. Emery, Comput. Methods Appl. Mech. Eng. 188 (2000) 217–233.
[3] D. Gabriel, J. Plesek, R. Kolman, F. Vales, J. Comput. Appl. Math. 234 (2010) 1930–1936.
[4] M.N. Guddati, B. Yue, Comput. Methods Appl. Mech. Eng. 193 (2004) 275–287.
[5] S. Krenk, Comput. Methods Appl. Mech. Engrg. 191 (2001) 975–987.
[6] K.J. Marfurt, Geophysics 49 (1984) 533–549.
[7] R. Mullen, T. Belytschko, Internat. J. Numer. Methods Engrg. 18 (1982) 11–29.
[8] G. Seriani, S.P. Oliveira, Geophysics 72 (2007) 95–106.
[9] G. Seriani, S.P. Oliveira, Wave Motion 45 (2008) 729–744.
[10] B. Yue, M.N. Guddati, J. Acoust. Soc. Am. 118 (2005) 2132–2141.
[11] F.I. Zyserman, P.M. Gauzellino, Finite Elem. Analysis and Design 41 (2005) 1309–1326.
[12] T. Hughes, A. Reali, G. Sangalli, Comput. Methods Appl. Mech. Engrg. 197 (2008) 4104–4124.
[13] X. Li, T. Zhu, M. Zhang, G. Long, Comput. Phys. Comm. 181 (2010) 1850–1858.
[14] Z.C. He, A.G. Cheng, G.Y. Zhang, Z.H. Zhong, G.R. Liu, Internat. J. Numer. Methods Engrg. 86 (2011) 1322–1338.

[15] D. Wang, R. Tezaur, J. Toivanen, C. Farhat, Internat. J. Numer. Methods Engrg. 89 (2012) 403–417.
[16] I. Babuska, F. Ihlenburg, T. Strouboulis, S.K. Gangaraj, Internat. J. Numer. Methods Engrg. 40 (1997) 3883–3900.
[17] I. Babuska, T. Strouboulis, S.K. Gangaraj, C.S. Upadhyay, Comput. Methods Appl. Mech. Eng. 140 (1997) 1–37.
[18] A. Deraemaeker, I. Babuska, P. Bouillard, Internat. J. Numer. Methods Engrg. 46 (1999) 471–499.
[19] A. Idesman, M. Schmidt, J.R. Foley, Comput. Mech. 47 (2011) 555–572.
[20] A.V. Idesman, Comput. Mech. 40 (2007) 261–279.
[21] A.V. Idesman, H. Samajder, E. Aulisa, P. Seshaiyer, Comput. Mech. 43 (2009) 797–814.
[22] A. Idesman, K. Subramanian, M. Schmidt, J.R. Foley, Y. Tu, R.L. Sierakowski, J. Sound Vib. 329 (2010) 2851–2872.
[23] A.V. Idesman, Comput. Model. Eng. Sci. 71 (2011) 111–148.
[24] A. Idesman, M. Schmidt, J.R. Foley, Wave Motion 48 (2011) 625–633.
[25] A.V. Idesman, D. Pham, Comput. Methods Appl. Mech. Eng. 271 (2014) 86–108.
[26] T. J. R. Hughes, The Finite Element Method: Linear Static and Dynamic Finite Element Analysis, Prentice- Hall, Englewood Cliffs, NJ, 1987.
[27] K.J. Bathe, Finite Element Procedures, Prentice-Hall Inc., Upper Saddle River, New Jersey, 1996.
[28] O.C. Zienkiewicz, R.L. Taylor, The Finite Element Method, Butterworth-Heinemann, Oxford, UK, 2000.
[29] G.M. Hulbert, T. J. R. Hughes, Comput. Methods Appl. Mech. Eng. 84 (1990) 327–348.
[30] A.V. Idesman, Compos. Struct. (2014) 1–20, submitted for publication.
[31] G. Gazonas, A. Velo, Wave Motion 49 (2012) 135–151.